Mass Detection Using a Texture Feature Coding Method

Ping-Sung Liao[1], Shu-Mei Guo[2], Yu-China Liao[2], Sheng-Chih Yang[3], Ching-Wen Yang[4], Hsiang-Ming Chen[5], Pau-Choo Chung[3], San Kan Lee[5,6], and Chein-I Chang[7]

Summary. Detection of masses is much more difficult than that of microcalcifications (MCCs) because breast masses are part of tissues that may not be detected effectively by the techniques developed for detection of MCCs. In this chapter, we present a texture feature coding method (TFCM) to extract features that could characterize special properties of masses. It extracts gradient variations of gray level co-occurrence matrix as texture features. As a result, the TFCM is more sensitive to changes in texture. Three neural network architectures, backpropagation neural network, probabilistic neural network, and radial basis function neural network are used for mass detection with inputs provided by TFCM-extracted features. The experimental results show that our TFCM-based neural network approaches can achieve a detection rate of approximately 87% with a 10% false alarm rate.

Key words. Gray level co-occurrence matrix, Mass detection, Texture feature coding method (TFCM), Texture spectrum (TS)

Introduction

The mortality and incidence of breast cancer for women in Taiwan is currently increasing. Hence, to prevent the worst cases of breast cancer happening in women is an important discipline for the Ministry of health and hospitals. Mammography is a

[1] Department of Electrical Engineering, Cheng Shiu Institute of Technology, 840 Chengching Road, (A33) Niaosung, Kaohshung, Taiwan, Republic of China
[2] Department of Information Engineering, National Cheng Kung University, Tainan 70101, Taiwan, Republic of China
[3] Department of Electrical Engineering, National Cheng Kung University, Tainan 70101, Taiwan, Republic of China
[4] Computer Center, Taichung Veterans General Hospital, Taichung, Taiwan, Republic of China
[5] Department of Radiology, Taichung Veterans General Hospital, Taichung 40705, Taiwan, Republic of China
[6] Department of Diagnostic Radiology, National Defense Medical Center, Taipei 100, Taiwan, Republic of China
[7] Remote Sensing Signal and Image Processing Laboratory, Department of Computer Science and Electrical Engineering, University of Maryland, Baltimore County, Baltimore, MD 21250, USA

useful screening tool recommended for early detection of suspicious regions of breast cancer by the American Cancer Society. The major symptom of breast cancer is either microcalcifications or masses as shown on mammograms. However, mass detection is much more difficult than that of microcalcifications because masses are part of breast tissues and the appearance of breast parenchyma is more complicated than that of MCCs. In particular, the intensity and contrast of masses are not easily characterized by a robust model. Because the spatial gray level dependence method (SGLDM) has been widely used in mass detection and classification [1–3], in this chapter, we propose a new SGLDM-based approach, referred to as the texture feature coding method (TFCM) [4, 5], to detect the existence of masses. TFCM extracts derivative features, referred to texture feature numbers (TFNs) from a spatial gray level co-occurrence matrix, and these TFNs could describe successive gradient changes in gray level among three consecutive pixels using the concepts of 4-neighbor connectivity and 8-neighbor connectivity. Therefore, the TFCM could be considered as a second-order SGLDM, and its feature vector associated to a suspicious region in a mammogram is chosen as the input in three neural network architectures for mass detection.

Texture Feature Coding Method

Let an image be of size $M \times N$ with $I(l, k)$ being the gray level of the pixel at the spatial location (l, k). The gray level co-occurrence matrix $N_{d,\theta}(i, j)$ denotes the number of transitions between two pixels whose gray levels are i and j with d-pixel apart and angular rotation θ. Normalizing $N_{d,\theta}(i, j)$ yields the probability of gray level transitions between i and j:

$$p(i, j \mid d, \theta) = \frac{N_{d,\theta}(i, j)}{\sum_{i,j} N_{d,\theta}(i, j)} \tag{1}$$

Using Eq. 1, the co-occurrence matrix specified by displacement d and angular orientation θ is defined by $\mathbf{W}_{d,\theta} = [p(i, j \mid d, \theta)]$.

For a 3×3 window mask over a pixel, there are eight orientations, 0°, 45°, 90°, 135°, 180°, 225°, 270°, and 315° as shown in Fig. 1a. According to the definition given in earlier reports [4, 5], the 4-neighbor connectivity of the pixel is described in Fig. 1b by four pixels labeled by 1, 3, 5, 7, and the other four pixels in the 8-neighbor connectivity labeled by 2, 4, 6, 8, as shown in Fig. 1c.

The idea of the TFCM is to consider three consecutive pixels along with certain specific directions and calculate gradient changes in gray levels of two successive adjacent pixels among these three pixels. Two directions are of interest, three pixels aligned in a perpendicular or diagonal direction. In the former case, the three pixels are first-order neighboring pixels connected by two perpendicular lines specified by 0°–180° and 90°–270° as shown in Fig. 1b, whereas in the latter case, the three pixels are second-order neighboring pixels connected by two diagonal lines specified by 45°–225° and 135°–315° in Fig. 1c. If we denote three consecutive pixels by their spatial coordinates at a, b, c and associated gray levels by $I(a)$, $I(b)$, and $I(c)$ respectively, the difference between the gray intensity in the center $I(b)$ and that of its neighborhood $I(b)$ and $I(c)$ may indicate the degree of roughness along a specified line. Let Δ be a desired

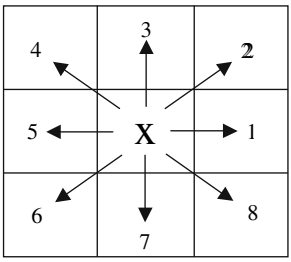

(a) 8 orientations

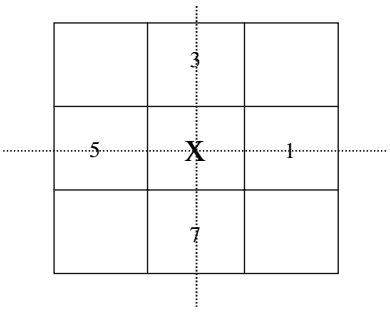

(b) first-order 4-neighbor connectivity

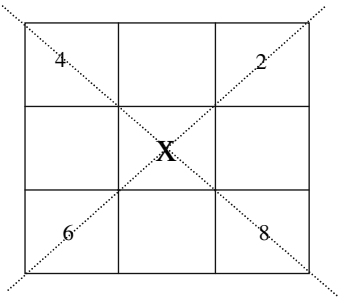

(c) second-order 4-neighbor connectivity

FIG. 1. 8-neighbor connectivity

gray level tolerance. Thus four types of successive gradient changes in gray level along the corresponding direction are defined below:

$$\text{(Type 1)} \left| I(a) - I(b) \right| \le \Delta, \left| I(b) - I(c) \right| \le \Delta$$

$$\text{(Type 2)} \left| I(a) - I(b) \right| \le \Delta, \left| I(b) - I(c) \right| > \Delta \text{ or } \left| I(a) - I(b) \right| > \Delta, \left| I(b) - I(c) \right| \le \Delta$$

$$\text{(Type 3)} I(a) - I(b) > \Delta, I(b) - I(c) > \Delta \text{ or } I(b) - I(a) > \Delta, I(c) - I(b) > \Delta$$

$$\text{(Type 4)} I(a) - I(b) > \Delta, I(c) - I(b) > \Delta \text{ or } I(b) - I(a) > \Delta, I(b) - I(c) > \Delta$$

According to degrees of successive gradient changes in gray level among three consecutive pixels, type 1 corresponds to zero-order variation because there are no gradient changes in gray level of two successive adjacent pixels, type 2 represents first-order variation because there is one gradient change in gray level that occurs in only one pair of two adjacent pixels, and type 3 and type 4 describe second-order variation because there are drastic gradient changes in gray level among three pixels.

Let $\alpha 1$ (0°–180° line), $\beta 1$ (90°–270° line), $\alpha 2$ (45°–225° line), and $\beta 2$ (135°–315° line) denote line types on which the three consecutive pixels are aligned respectively. As a result, each parameter of $\alpha 1$, $\alpha 2$, $\beta 1$, and $\beta 2$ takes values from {1, 2, 3, 4} where a number i represents type (i) of successive gradient variation. For each pixel of an image, its TFN is derived by Eq. 2 as below:

$$TFN(x, y) = \alpha(x, y) \times \beta(x, y) \tag{2}$$

where $\alpha(x, y)$ equals to $\alpha 1(x, y)$ times $\alpha 2(x, y)$, and $\beta(x, y)$ equals to $\beta 1(x, y)$ times $\beta 2(x, y)$. Obviously, there are 256 possible combined types of successive gradient variations. However, by reindexing after removing the illegal cases, the number of all reasonable cases is 41 [4, 5]. Furthermore, based on the histogram of texture feature number, we define several one-dimensional (1D) TFN descriptors such as coarseness, homogeneity, mean convergence, and variance as 1D features for mass detection [6].

Similar to the co-occurrence matrix in SGLDM, the TFN co-occurrence matrix is defined in Eq. 3:

$$W_{TFN_{\Delta^*,d,\theta}}(i,j) = \sum_{l=1}^{M}\sum_{k=1}^{N} \delta_{TFN_{\Delta^*,d,\theta}}(l,k) \tag{3}$$

where $0 \le i \le 40$, $0 \le j \le 40$, and optimal tolerance Δ^* is set to 3 in our experiment.

$$\delta_{TFN_{\Delta^*,d,\theta}}(l,k) = \begin{cases} 1 & \text{if } TFN_{\Delta^*}(l,k) = i, TFN_{\Delta^*}(l + d\cos\theta, k + d\sin\theta) = j \\ 0 & \text{otherwise} \end{cases} \tag{4}$$

Normalizing the Eq. 3 of the TFN co-occurrence matrix yields the probability function of TFN co-occurrence matrix:

$$P_{TFN_{\Delta^*,d,\theta}}(i,j) = \frac{W_{TFN_{\Delta^*,d,\theta}}(i,j)}{\sum_{i=0}^{41}\sum_{j=0}^{41} W_{TFN_{\Delta^*,d,\theta}}(i,j)} \tag{5}$$

Next, like 1D TFN descriptors, we also define three two-dimensional (2D) TFN descriptors such as entropy, similarity, and regularity as 2D features for mass detection [6]. As a result, these 1D texture descriptors and 2D texture descriptors are packed together as a feature vector that could describe the gray variations in a suspicious region in a mammogram. Certainly, this feature vector will be fed into the input nodes of neural networks being briefly introduced in the next section.

Three neural network architectures, probabilistic neural network (PNN), radial basis function neural network (RBFNN), and backpropagation neural network (BPNN) are proposed in this section for mass detection. The basic concept of PNN roots in statistical Bayesian classifier using Gaussian distributions. It is a network with no need of training [7]. The BPNN is a three-layer neural network with its performance completely determined by training samples with backpropagation as the training algorithm [8]. The RBFNN is also a three-layer neural network and implements a hidden layer with the hidden nodes being the training samples using Gaussian kernels as activation functions [8].

Experiments and Discussion

In our experiments, the MIAS MiniMammographic Database [9] provided by the Mammographic Image Analysis Society (MIAS) is used. There are 207 normal mammograms compared to 115 mammograms that contain abnormal tissues. Three classes are considered in accordance with breast parenchyma—dense-glandular, fatty, and fatty-glandular. Among 207 normal mammograms there are 76 dense-glandular, 66 fatty, and 65 fatty-glandular. For each mammogram of dense-glandular, fatty, and

fatty-glandular, we randomly pick up three regions with size 65×65 pixels as the normal tissues for training and classification. As to 115 abnormal mammograms, there are 23 dense-glandular, 35 fatty, and 29 fatty-glandular.

To evaluate the effectiveness of mass detection, we consider the following three parameters as performance measures:

1. Detection rate: $DR = TPN/N_p$
2. False alarm rate: $FAR = FPN/N_n$
3. Correct classification rate: $CR = (TPN + TNN)/(N_p + N_n)$

where TPN is the number of masses detected among total tumor tissues, FNN is the number of failures to detect mass among total tumor tissues, TNN is the number of normal cases detected as normal tissues, FTN is the number of failures to detect masses among total normal tissue, N_p is the number of abnormal cases with masses, and N_n is the number of normal tissue cases.

When all 1D texture descriptors and 2D texture descriptors are computed, they are first normalized into [0–1] to prevent from overflow during computation in classification. As for abnormal breast tissues, we randomly chose 12 dense-glandular, 18 fatty, and 15 fatty-glandular as the training samples with the rest used as text images. Similarly, to the normal tissues were randomly and evenly divided into two groups, one for training samples and another for test samples.

Because there are too few real cases to validate our proposed texture feature coding method in conjunction with three neural network platforms, our experiments were conducted as 100 iterations by randomly selecting the training samples and testing samples. The results are finally given by the means under 100 experiments. Table 1 tabulates the experimental results of detecting masses by using three different neural networks where TPN is true positive number, FNN is false negative number, TNN is true negative number, FPN is false positive number, DR is detection rate, FAR is false alarm rate, and CR is correct classification rate.

Table 1. Performance comparison under different neural networks

Backpropagation neural network (BPNN):							
Breast tissue	TPN	FNN	TNN	FPN	DR%	FAR%	CR%
Dense-glandular	9.17	1.83	187.68	28.32	83.36	13.11	86.72
Fatty	15.52	1.48	168.83	11.17	91.29	6.21	93.58
Fatty-glandular	11.88	2.12	161.31	18.69	84.86	10.38	89.27
Radial basis function neural network (RBFNN):							
Breast tissue	TPN	FNN	TNN	FPN	DR%	FAR%	CR%
Dense-glandular	6.97	4.03	153.44	62.56	63.36	28.96	70.67
Fatty	11.78	5.22	142.32	37.68	69.29	20.93	78.22
Fatty-glandular	8.6	5.4	128.74	51.26	61.43	28.48	70.79
Probabilistic neural network (PNN):							
Breast tissue	TPN	FNN	TNN	FPN	DR%	FAR%	CR%
Dense-glandular	9.31	1.69	189.71	26.29	84.64	12.17	87.67
Fatty	15.51	1.49	170.92	9.08	91.24	5.04	94.63
Fatty-glandular	12.18	1.82	159.3	20.7	87	11.5	88.39

From Table 1, the detection abilities of BPNN and PNN outperformed the RBFNN. Based on the obtained statistical means, BPNN could an achieve an approximate 86% detection rate with a false alarm rate 10% whereas the PNN could reach an approximate 87% detection rate with 10% false alarm rate.

Conclusion

In this chapter, TFCM is proposed to extract the gradient variations along two specific directions. The experimental results show that our TFCM-based neural network approaches can achieve an approximate 87% detection rate with a 10% false alarm rate. It implies that the texture feature from TFCM could effectively discriminate between abnormal and normal tissues in a mammogram.

Acknowledgments. This work is supported by a grant received from the Taichung Veterans General Hospital number TCVGH-915509C. The authors are grateful for the database provided by Mammographic Image Analysis Society (MIAS).

References

1. Chan HP, Wei D, Helvie MA, et al (1995) Computer-aided classification of mammographic masses and normal tissue: linear discriminant analysis in texture feature space. Phys Med Biol 40:857–876
2. Christoyianni I, Dermatas E, Kokkinakis G (1999) Neural classification of abnormal tissue in digital mammography using statistical features of the texture. ICECS99 1:117–120
3. Hadjiiski L, Sahiner B, Chan HP, et al (1999) Classification of malignant and benign masses based on hybrid ART2LDA approach. IEEE Trans Med Imaging 18:1178–1187
4. Chang CI (1995) Final report NSC-84-2213-E-006-086. National Science Council in Taiwan
5. Hong MH, Sung YN, Lin XZ (2002) Texture feature coding method for classification of liver sonography. Comput Med Imaging Graphics 26:33–42
6. Liao YC (2002) Mass detection using texture analysis. Master thesis, Department of Computer Science and Information Engineering, Chen Kung University, Taiwan
7. Specht DF (1990) Probabilistic neural networks and the polynomial adaline as complementary techniques for classification. IEEE Trans Neural Networks 1:111–121
8. Bishop CM (1995) Neural networks for pattern recognition. Oxford University Press, New York
9. The Mammographic Image Analysis Society, Digital Mammography Database. www.wiau.man.ac.uk/services/MIAS/MIASweb.html